

Unlocking Internal Prestress from Protein Nanoshells

W. S. Klug,¹ W. H. Roos,^{2,*} and G. J. L. Wuite²

¹*Department of Mechanical and Aerospace Engineering, and California NanoSystems Institute, UCLA, Los Angeles, California 90095, USA*

²*Natuur- en Sterrenkunde & LaserLab, VU University, De Boelelaan 1081, 1081 HV Amsterdam, Netherlands*
(Received 18 October 2011; published 19 October 2012)

The capsids of icosahedral viruses are closed shells assembled from a hexagonal lattice of proteins with fivefold angular defects located at the icosahedral vertices. Elasticity theory predicts that these disclinations are subject to an internal compressive prestress, which provides an explanation for the link between size and shape of capsids. Using a combination of experiment and elasticity theory we investigate the question of whether macromolecular assemblies are subject to residual prestress, due to basic geometric incompatibility of the subunits. Here we report the first direct experimental test of the theory: by controlled removal of protein pentamers from the icosahedral vertices, we measure the mechanical response of so-called “whiffle ball” capsids of herpes simplex virus, and demonstrate the signature of internal prestress locked into wild-type capsids during assembly.

DOI: [10.1103/PhysRevLett.109.168104](https://doi.org/10.1103/PhysRevLett.109.168104)

PACS numbers: 87.80.Ek, 87.15.bk, 87.85.jc

Self-assembly of macromolecules is generically driven by an interplay between the geometry of the subunits and the attractive physical interactions between the subunits. Subtle tuning of this interplay, e.g., by mutation and/or modification of the chemical environment, can activate or block the assembly process, as in amyloid fibril assembly [1], or result in structural polymorphism, as in the assembly of the protein shells (capsids) of viruses [2,3]. Because of their robust assembly and regular icosahedral symmetry, spherical viral capsids have been an ideal system for exploring the physical principles governing macromolecular assembly. Coarse-grained molecular dynamics studies have shown that icosahedral capsid assembly can be successfully simulated through precise design of subunit interfaces and local assembly rules for smaller viruses [4–7]. However, as capsid size and the number of units grows, assembly simulations suffer a “closure catastrophe,” becoming kinetically trapped in “monster particle” states, i.e., misassembled aggregates and open shells [5]. Thus, the key question remains open: beyond local rules, what are the physical mechanisms that guide or control the assembly of large macromolecular aggregates?

Lidmar, Mirny, and Nelson (LMN) approached this question building onto the framework of continuum theory of thin elastic shells [8]. They describe how pentamers located on fivefold icosahedral vertices are predicted to behave as defects (disclinations) in an otherwise hexahedral lattice of capsid proteins. According to elasticity theory, these defects inject a state of prestress into the shell, because the naturally sixfold coordinated subunits are geometrically incompatible with the fivefold vertex topology. The resulting strain causes the icosahedral vertices to “buckle” outward, and for larger viruses this leads to a faceted, aspherical capsid shape. Yet, the elastic energy cost of inserting a pentamer at the proper location

of an icosahedral vertex of a growing shell is always higher than the cost of inserting a hexamer, as recently shown by Morozov *et al.* [9]. This leads to the suggestion that so called “whiffle ball” capsids [10], with the 12 pentamers missing, might serve as assembly intermediates, which are then subject to pentamer insertion as a final assembly step. While such an assembly pathway might be plausible for smaller capsids, the cost of a disclination increases with capsid size, making pentamer addition as a final step prohibitive in sufficiently large capsids. Thus the fact that large, highly faceted viruses do spontaneously assemble prompts the question of whether their capsids might relax the defect-induced prestress,

To address the general question of the presence and impact of prestress on macromolecular assemblies, we perform quantitative experimental testing of the elasticity theory of viruses, and assess whether capsids are indeed subject to incompatibility-driven prestress. Because the internal state of stress or force in a capsid shell is not directly measurable, we consider instead an alternative approach. We assess the amount of prestress in a viral shell indirectly by comparing the measured mechanical properties of native capsids with those of whiffle ball capsids [10,11], which are indistinguishable from the former except that they lack pentons [Fig. 1(a)]. Following the LMN theory [8], we model the capsids as elastic icosahedral shells, with an energy functional

$$F = \int \frac{\kappa}{2} (2H)^2 dA + \int \left(\frac{\lambda}{2} E_{kk}^2 + \mu E_{ij} E_{ij} \right) dA,$$

with bending contributions from the mean curvature H and stretching contributions from the (nonlinear) Green strain E_{ij} , defined relative to the icosahedral reference state. The most notable consequence of the prestressed disclinations is a “buckling” transition controlled by a single

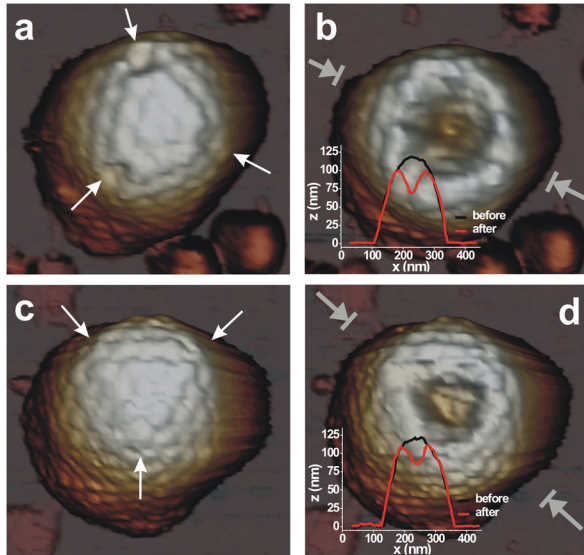


FIG. 1 (color). HSV1 B capsids deposited on their threefold symmetry axis. The top AFM images (a),(b) are from a whiffle ball capsid and the bottom images (c),(d) are from an intact particle. The capsids are shown in a 3D-perspective rendering and the white arrows in (a),(c) indicate the icosahedral vertices. One can see three holes in image (a) at the places where the pentamers are removed. The particles are shown before (a),(c) and after (b),(d) nanoindentation. The insets in (b),(d) show the height profile (as taken along the gray arrows) before and after indentation, where x denotes the lateral distance and z the particle height.

dimensionless parameter, the Föppl–von Kármán (FvK) number, $\gamma = YR^2/\kappa$, representing the ratio of in- and out-of-plane stiffnesses of the shell in terms of the 2D Young’s modulus Y (common scaling factor for 2D Lamé coefficients λ and μ), bending modulus κ , and shell radius R [8]. This transition is manifested in an abrupt increase of the asphericity of the shell, $\langle(R - \langle R \rangle)^2\rangle/\langle R \rangle^2$, from zero to a finite value as γ is increased above a threshold value $\gamma \approx 150$. Because pentons represent disclination cores, it follows that their removal should reduce the prestress, and therefore the driving force for buckling of the icosahedral vertices. We obtain equilibrium configurations of both intact and whiffle ball shells by relaxation of the energy, computed numerically by finite-element approximation on triangular meshes, using C^1 -conforming subdivision-surface shape functions for bending, and Lagrange interpolation for stretching [12,13]. The triangular finite-element meshes were generated by recursive subdivision of the Caspar-Klug T -number triangulations, to obtain convergence to the continuum limit, which, for an intact shell, is insensitive to the base T number. Whiffle ball shells are assigned traction-free boundary conditions along the edges of penton holes, which are sized according to capsid base T number.

Figure 2 plots the asphericity vs γ of intact shells and $T = 16$, $T = 7$, and $T = 4$ whiffle ball shells, as computed

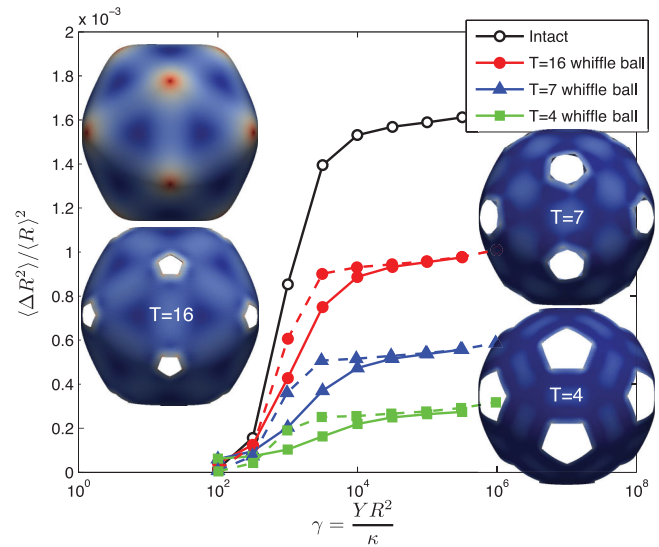


FIG. 2 (color). Asphericity as function of FvK number computed by finite-element analysis for “intact” (i.e., closed) and whiffle ball icosahedral elastic shells. Dashed lines show results using the shape of relaxed intact shells, but ignoring the pentons, i.e., making them “invisible.” Insets show the relaxed equilibrium shapes for shells having $\gamma = 1000$, with color contours indicating stretching energy density. Results for closed shells are marked intact. Whiffle ball shells are labeled by the Caspar-Klug T number defining the structure of the hexons and the removed pentons. For smaller T numbers the holes at the pentameric sites are larger in proportion to the average shell radius. For the analysis, the finite-element discretizations were refined to a sufficient level that the results were insensitive to further refinement.

by finite-element analysis (FEA). At fixed $\gamma \geq 150$ (above the buckling threshold) removal of pentons leads to a reduction in asphericity. The insets of Fig. 2 show the relaxed shape of shells with $\gamma = 1000$ contoured by the strain energy density. The figure demonstrates the predicted decrease in asphericity for the whiffle balls, seemingly indicating that the softening of the buckling transition induced by penton removal is associated with a reduction in the internal stresses in the shell. However, if one determines the asphericity of the intact capsids *without* taking into account the presence of the pentons (dashed lines in Fig. 2) one sees that the difference between intact capsids with “invisible” pentons and whiffle balls vanishes for most regimes. Examination of cryoelectron microscopy reconstructions of three experimentally observed whiffle ball capsids of the $T = 16$ herpes simplex virus type 1 (HSV1) and the $T = 7$ capsids of HK97 and P22, all of which are identical from native capsids except that they have holes at the 12 icosahedral vertices [10,14,15], shows a seemingly qualitative agreement with the prediction that whiffle ball capsids are less faceted than their intact counterparts. However, as with the simulations, also here there

is a catch as difference maps between P22 intact and whiffle ball capsids predominantly show differences at the location of the missing pentons, not at the hexons [14]. These combined results reveal that change in shape after penton removal is inconclusive as a gauge for prestress.

As an alternative experimental test of the prediction of prestress, we assess instead the effect of penton removal on the global mechanical properties of capsids. Specifically, we performed atomic force microscopy (AFM) nanoindentation experiments [16,17] on intact and whiffle ball capsids of HSV1, as described previously (see [18] for materials and methods) [19]. The individual indentation curves and their average are shown in Fig. 3. From the initial deformation, we measure spring constants of 0.174 ± 0.002 N/m for the whiffle ball capsids and 0.35 ± 0.01 N/m for the intact capsids (errors are standard error of the mean, SEM). The large (irreversible) drops in the force mark failure events. The general trend is that whiffle ball particles show a more catastrophic failure than intact capsids. The relative drop in the force is $55 \pm 7\%$ for the whiffle ball capsids whereas it is $39 \pm 8\%$ for the intact capsids. The larger drops in force for the whiffle balls are also accompanied by larger holes remaining after nanoindentation (Fig. 1).

In comparing the experimental data to FEA we choose a FvK number of 1500 as representative of the contiguous shell of a HSV1 capsid [16]. Figure 4 shows the indentation behavior predicted by theory for intact and whiffle ball particles. The main graph shows force-indentation curves

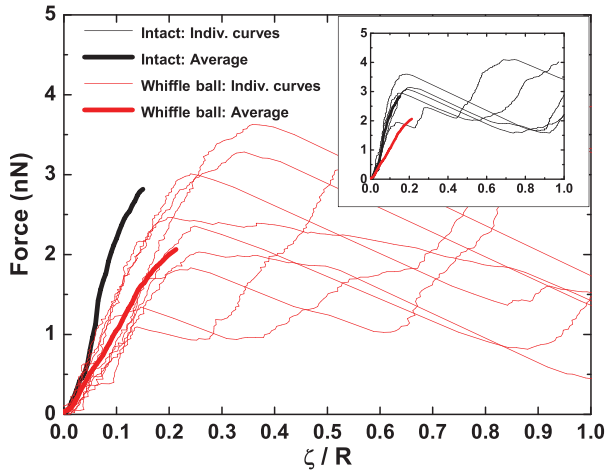


FIG. 3 (color). Indentation curves (thin lines show individual curves) and their averages (thick lines) for whiffle ball $T = 16$ capsids (number of particles $n = 9$) and intact $T = 16$ capsids ($n = 5$, inset) along the threefold symmetry axis. Both averages are shown in both graphs; only the beginning of these curves are shown. The negative slope following on failure of most particles is ~ 0.05 N/m, which equals the spring constant of the used cantilever and represents the relaxation of the cantilever after a breaking event.

of icosahedral particles using the LMN theory, which allows for prestresses due to the disclinations [8]. The “intact” curve is for a closed icosahedral shell (no holes), and the $T = 16$, 7, and 4 cases are shells without pentamers, with holes that are relatively larger for smaller T numbers. Three similarities of the theoretical and experimental curves (Fig. 3) are apparent: (i) the critical force at which the particle buckles or fails is for whiffle ball particles lower than for intact particles, (ii) the indentation at the critical force for whiffle ball particles is higher than for intact particles, (iii) after an initial similar linear deformation (up to an indentation of $\sim 5\%$ of the particle radius), the intact capsids stiffen whereas the whiffle ball capsids deform nearly linearly, up to the critical force. Equating the experimental stiffness values to the model with $\gamma = 1500$ and $R = 49.5$ nm [16], we extract values of $Y = 3200$ pN/nm and $\kappa = 5300$ pN nm for the intact capsid and $Y = 2400$ pN/nm and $\kappa = 4000$ pN nm for the whiffle ball shell. Assuming an effective mechanical thickness of $h = 4$ nm we obtain 3D Young’s moduli of $E = Y/h = 0.80 \pm 0.02$ GPa for intact capsids and $E = 0.60 \pm 0.01$ GPa for the whiffle ball (as indication shown with the same relative errors as for the experimentally obtained spring constant). This value for the intact capsids is close to previous estimations of E [18]. Furthermore, it shows that the experimentally observed decrease in spring

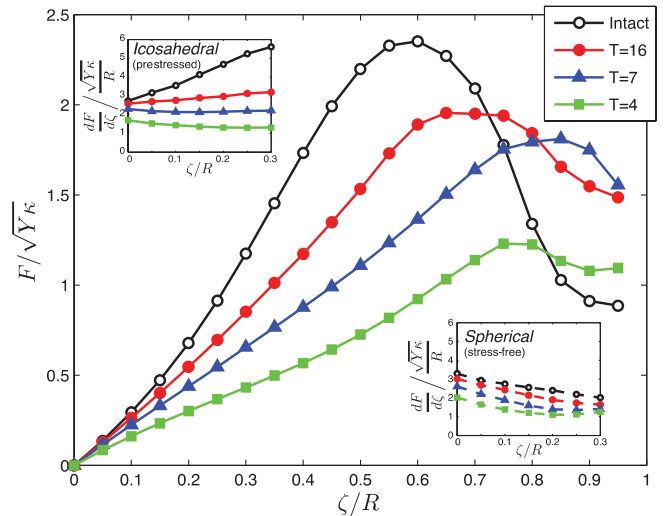


FIG. 4 (color). Normalized, simulated force-indentation responses of intact and whiffle ball icosahedral (prestressed) shells with $\gamma = 1500$. Whiffle ball shells with triangulation numbers $T = 16$, $T = 7$, and $T = 4$, have structures depicted in Fig. 2. Indentation loading was oriented along the threefold symmetry axis of the shells. The top left inset shows normalized stiffnesses, i.e., the derivatives of the curves in the main plot, corresponding to prestressed icosahedral shells. The bottom right inset shows the stiffness curves for shells with spherical (stress-free) reference states, revealing dramatically smaller differences between intact and whiffle ball shells than are seen for prestressed icosahedral shells.

constant going from intact to whiffle ball is reflected by the decrease in modulus in the simulations. However, it is not *a priori* obvious that the moduli will be affected by penton removal and these results yield that the whiffle ball capsids as measured by experiment are 25% softer than would be predicted by the model if the elastic moduli were unaffected by penton removal. This decrease in intrinsic stiffness will be related to the fact that upon experimental penton removal, also some of the triplex proteins that connect the capsomeres in HSV1 are removed, specifically those that are immediately adjacent to the pentons [15]. This triplex removal effectively increases the size of the hole at the vertex. By comparing Figs. 2 and 4 one can see that the simulations predict a consistent trend: a larger drop in elastic stiffness for larger holes at the vertices. In addition, one can observe in the curves that the experimental shells fail before the simulated shells buckle. This resembles the effect of imperfections in premature initiation of buckling failure of macroscopic structures [20]; however, quantitative comparisons of buckling or failure remain suspect as we do not have a clear justification for interpreting the experimental failure as a buckling transition.

While agreement with the experimental data provides a measure of validation for the elasticity theory, it does not yet cleanly identify *prestress* as the direct cause for the reduced stiffness of the whiffle ball shells. For a rigorous test of the presence of prestressed disclinations in icosahedral shells we also examine the predictions of elasticity theory for spherical whiffle ball shells without prestress. The insets in Fig. 4 show the normalized or structural stiffness, i.e., the derivative of the force-indentation curves, $\frac{dF}{d\zeta} / \frac{\sqrt{Y\kappa}}{R}$, for icosahedral (prestressed) and for spherical (stress-free) shells. It demonstrates that the reduction in structural stiffness, averaged over the range $0 \leq \zeta \leq R$, for initially stress-free shells is significantly smaller ($< 10\%$) than for shells with initial prestress ($\approx 35\%$). This is in large part due to the nonlinear force response of intact shells: stress-free shells soften as indentation is increased, while prestressed shells stiffen consistent with the experiments. These results provide strong support for the conclusion that prestress does indeed exist in $T = 16$ HSV1 capsids. If HSV1 were stress free, the $T = 16$ shell model would predict that penton removal would lead to such a small change in stiffness so as to be unobservable to within experimental accuracy. Figure 3 shows a clear effect of penton removal and the actual experimental reduction in spring constant is $\sim 50\%$. The model also predicts a large change in structural stiffness: 35%. This structural difference in stiffness is normalized on the relevant elastic parameters; i.e., this is the change in stiffness which would occur when Y , κ , and E do not change. However, the experimental results show a bigger change, indicating that the intrinsic stiffness (i.e., Y , κ , and E) is also changing. By comparing the model with the experiments, we

have, in the previous section, observed a 25% reduction in the elastic modulus. So putting things together we now have a reduction of 25% in intrinsic stiffness and 35% in structural stiffness going from intact capsids to whiffle balls. As the intrinsic and structural stiffness couple into the overall stiffness k , as measured experimentally, this yields the 50% reduction in spring constant we observe in the nanoindentation experiments. To conclude this section, we have shown that the large experimental change in stiffness is consistent with a prestressed $T = 16$ shell model, and inconsistent with a stress-free spherical $T = 16$ model.

Our current findings described here stand in apparent contrast to a previous study of the mechanical properties of capsids of a smaller virus, hepatitis B virus (HBV), which assemble *in vivo* as well as *in vitro* with triangulation numbers of either $T = 3$ or $T = 4$. Comparison of theory and experiment for HBV suggested that the anisotropy or orientation dependence of the indentation response was inconsistent with prestresses at the fivefold disclinations [21], raising a challenge for the predictions of elasticity theory as applied to smaller viruses. Because individual protein dimensions and interactions tend to persist within a narrow range of values across the spectrum of virus families, smaller capsids tend to have smaller FvK numbers, and should therefore, according to theory, have correspondingly more spherical shapes. The Föppl-von Kármán number of HBV was estimated to be less than 400 [21], close to the buckling transition. Figure 2 shows that the large differences between intact and whiffle balls are only prominent above $\gamma \sim 500$. This illustrates an important distinction: while prestress is important for producing the aspherical shapes of large FvK viruses, it is more or less irrelevant for small capsids. The mechanical properties of the latter class, for instance HBV, are more likely to be governed by the discreteness of the protein shell [21]. As capsid size gets larger, prestress has an increasingly more dominant role in determining the mechanical properties as it affects the overall morphology.

By selectively removing the pentons of icosahedral viral shells and comparing their mechanical properties to intact shells we have experimentally validated the LMN theory on the presence of prestress. Especially for large viruses this prestress is apparent showing that their assembly process is unlikely to occur via a whiffle ball intermediate state as that would require the pentons to be in a relaxed state to avoid large energy penalties during self-assembly. Alternative assembly pathways, for instance starting with a nucleus of fivefold symmetry as recently observed for HBV and Norwalk virus [22], could also apply for larger T -number capsids as this would lock in the prestress from the start of assembly.

W.H.R. and G.J.L.W. acknowledge support from a NanoSci-E⁺ grant and the Stichting voor Fundamenteel Onderzoek der Materie (FOM) under the ‘‘Physics of the Genome’’ research program to GJLW. W.S.K. was

supported by NSF Grants No. CMMI-0748034 and No. DMR-1006128. We thank Kerstin Radtke and Beate Sodeik (Medizinische Hochschule Hannover) for providing the HSV1 capsids. We thank Robijn Bruinsma (UCLA) for the suggestion to initiate this study.

*Corresponding author.

wroos@few.vu.nl

- [1] S. Zibac, G. Fraser, R. Jakes, D. Owen, L. C. Serpell, R. A. Crowther, and M. Goedert, *J. Biol. Chem.* **285**, 38 555 (2010).
- [2] A. Zlotnick, N. Cheng, J. F. Conway, F. P. Booy, A. C. Steven, S. J. Stahl, and P. T. Wingfield, *Biochemistry* **35**, 7412 (1996).
- [3] L. Lavelle, M. Gingery, M. Phillips, W. M. Gelbart, C. M. Knobler, R. D. Cadena-Nava, J. R. Vega-Acosta, L. A. Pinedo-Torres, and J. Ruiz-Garcia, *J. Phys. Chem. B* **113**, 3813 (2009).
- [4] M. F. Hagan and D. Chandler, *Biophys. J.* **91**, 42 (2006).
- [5] H. D. Nguyen, V. S. Reddy, and C. L. Brooks, *Nano Lett.* **7**, 338 (2007); A. Luque, D. Reguera, A. Morozov, J. Rudnick, and R. Bruinsma, *J. Chem. Phys.* **136**, 184507 (2012).
- [6] D. C. Rapaport, *Phys. Rev. Lett.* **101**, 186101 (2008).
- [7] M. F. Hagan, *Phys. Rev. E* **77**, 051904 (2008).
- [8] J. Lidmar, L. Mirny, and D. R. Nelson, *Phys. Rev. E* **68**, 051910 (2003).
- [9] A. Morozov *et al.*, in *Emerging Topics in Physical Virology*, edited by P. Stockley and R. Twarock (Imperial College Press, London, 2010).
- [10] Y. Li, J. F. Conway, N. Cheng, A. C. Steven, R. W. Hendrix, and R. L. Duda, *J. Mol. Biol.* **348**, 167 (2005).
- [11] W. W. Newcomb and J. C. Brown, *J. Virol.* **65**, 613 (1991).
- [12] W. S. Klug, R. F. Bruinsma, J.-P. Michel, C. M. Knobler, I. L. Ivanovska, C. F. Schmidt, and G. J. L. Wuite, *Phys. Rev. Lett.* **97**, 228101 (2006).
- [13] L. Ma and W. S. Klug, *J. Comput. Phys.* **227**, 5816 (2008).
- [14] C. M. Teschke, A. McGough, and P. A. Thuman-Commike, *Biophys. J.* **84**, 2585 (2003).
- [15] W. S. Newcomb, B. L. Trus, F. P. Booy, A. C. Steven, J. S. Wall, and J. C. Brown, *J. Mol. Biol.* **232**, 499 (1993).
- [16] W. H. Roos, R. Bruinsma, and G. J. L. Wuite, *Nat. Phys.* **6**, 733 (2010).
- [17] I. L. Ivanovska, P. J. de Pablo, B. Ibarra, G. Sgalari, F. C. MacKintosh, J. L. Carrascosa, C. F. Schmidt, and G. J. L. Wuite, *Proc. Natl. Acad. Sci. U.S.A.* **101**, 7600 (2004).
- [18] W. H. Roos, K. Radtke, E. Kniesmeijer, H. Geertsema, B. Sodeik, and G. J. L. Wuite, *Proc. Natl. Acad. Sci. U.S.A.* **106**, 9673 (2009).
- [19] In contrast to the typical approach to only analyze the particles before indentation [17,18], we now explicitly analyze the particles before and after indentation. Only those particles that have a defined orientation before indentation and that show a clear hole in the middle of the particle after indentation are taken into account (Fig. 1). This method assures that (i) the proper orientation of the icosahedral particle is assessed and (ii) the indenting force is exerted at the middle of the viral shell and not off axis.
- [20] C. R. Calladine, *Theory of Shell Structures* (Cambridge University Press, Cambridge, 1983).
- [21] W. H. Roos *et al.*, *Biophys. J.* **99**, 1175 (2010).
- [22] C. Uetrecht, I. M. Barbu, G. K. Shoemaker, E. van Duijn, and A. J. R. Heck, *Nat. Chem.* **3**, 126 (2011).